An Analytical Model of Divisive Normalization in Disparity-Tuned Complex Cells

W. Stürzl[1], H.A. Mallot[2], and A. Knoll[1]

[1] Robotics and Embedded Systems, Technical University of Munich, Germany
[2] Cognitive Neuroscience, University of Tübingen, Germany
stuerzl@in.tum.de

Abstract. Based on the energy model for disparity-tuned neurons, we calculate probability density functions of complex cell activity for random-dot stimuli. We investigate the effects of normalization and give analytical expressions for the disparity tuning curve and its variance. We show that while normalized and non-normalized complex cells have similar tuning curves, the variance is significantly lower for normalized complex cells, which makes disparity estimation more reliable. The results of the analytical calculations are compared to computer simulations.

1 Introduction to the Binocular Energy Model

An overview of the binocular energy model [1] and an extension consisting of an additional normalization operation is shown in Fig. 1. The model is motivated by neurophysiological recordings from disparity-tuned neurons in the visual cortex of mammals. It is similar to the spatio-temporal energy model for motion perception described in [2].

In the first stage, left and right images, $I_l(x, y)$ and $I_r(x, y)$ respectively, are convolved with pairs of orthogonal filters,

$$S_{al} = \iint f_{al}(\xi,\eta)\, I_l(\xi,\eta)\, d\xi d\eta \ , \quad S_{ar} = \iint f_{ar}(\xi,\eta)\, I_r(\xi,\eta)\, d\xi d\eta \ , \tag{1}$$

$$S_{bl} = \iint f_{bl}(\xi,\eta)\, I_l(\xi,\eta)\, d\xi d\eta \ , \quad S_{br} = \iint f_{br}(\xi,\eta)\, I_r(\xi,\eta)\, d\xi d\eta \ . \tag{2}$$

The linear receptive fields defined by the functions $f_{al}, f_{bl}, f_{al}, f_{bl}$ can be modelled as Gabor functions, see e.g. [3],

$$G(\boldsymbol{x}-\boldsymbol{x}_0|\boldsymbol{k},\hat{\boldsymbol{\Sigma}},\phi) = e^{-\frac{1}{2}(\boldsymbol{x}-\boldsymbol{x}_0)^\top \hat{\boldsymbol{\Sigma}}^{-1}(\boldsymbol{x}-\boldsymbol{x}_0)} \cos(\boldsymbol{k}^\top(\boldsymbol{x}-\boldsymbol{x}_0)-\phi) \ . \tag{3}$$

$\boldsymbol{x}_0$ denotes the center position of a simple cell's receptive field in the image or retina, $\boldsymbol{k}$ determines the spatial frequency and the orientation. The monocular receptive fields have a phase difference of 90°, i.e. $\phi_{bl} = \phi_{al} + \frac{1}{2}\pi$, $\phi_{br} = \phi_{ar} + \frac{1}{2}\pi$.

Binocular simple cells combine the corresponding left and right filter responses (see Fig. 1),

$$S_a = S_{al} + S_{ar} \ , \quad S_b = S_{bl} + S_{br} \ , \tag{4}$$

J. Marques de Sá et al. (Eds.): ICANN 2007, Part I, LNCS 4668, pp. 776–787, 2007.

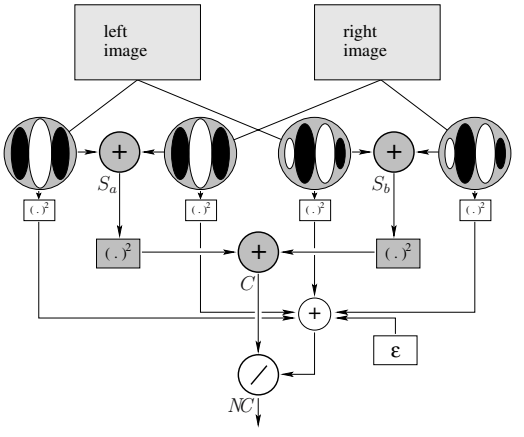

Fig. 1. Overview of the binocular energy model. The "classical" model, Eqs. (1)–(5), is depicted as gray panels. The white panels show the additional operations of the normalization step, Eq. (6). See text for details.

and output the squared sum to the complex cell. Mathematically equivalent but biologically more plausible, one can use four units instead, that have sign-inverted receptive fields and a half-squaring non-linearity [4].

Finally, binocular complex cells integrate responses of (at least) two simple cells,

$$C = S_a^2 + S_b^2 \ . \tag{5}$$

Binocular Normalization

The "classical" energy model has been extended by adding monocular and binocular divisive normalization operations [5]. In this paper, we will examine the effect of binocular normalization as depicted in Fig. 1. We define a normalized complex cell by

$$\mathcal{NC} := \frac{C}{(S_{al}^2 + S_{ar}^2 + S_{bl}^2 + S_{br}^2) + \varepsilon} = \frac{S_a^2 + S_b^2}{(S_{al}^2 + S_{ar}^2 + S_{bl}^2 + S_{br}^2) + \varepsilon} \ . \tag{6}$$

$\varepsilon \geq 0$ is a small normalization constant. For high local image contrast (estimated by $S_{al}^2 + S_{ar}^2 + S_{bl}^2 + S_{br}^2$) the effect of ε is negligible. Eq. (6) is a simple variant of the binocular normalization model proposed in [5] which enables us to show analytically, that the variance of normalized complex cell activity is reduced, and disparity detection is thus enhanced.

Similar models for "divisive normalization" or "gain control" have been used to describe several properties of visual cortex neurons, like response saturation and cross-orientation inhibition [6,7,8].

2 Probability Density Functions for Complex Cells

In this section, we will calculate probability density functions, tuning curves and variances of disparity-tuned complex cells of the "classical" energy model (which

we will call "non-normalized complex cells"), and of normalized complex cells defined in Eq. (6). We will assume random dot stereo images as stimuli.

2.1 Receptive Field Functions of the Position-Shift Type

In the following, we will consider vertically oriented receptive field functions, i.e. we set $\boldsymbol{k} = k\,\boldsymbol{e}_x$ and $\hat{\boldsymbol{\Sigma}} = \mathrm{diag}(\sigma_x^2, \sigma_y^2)$ in Eq. (3),

$$G(\boldsymbol{x} - \boldsymbol{x}_0 | k, \sigma_x^2, \sigma_y^2, \phi) = e^{-\frac{(x-x_0)^2}{2\sigma_x^2} - \frac{(y-y_0)^2}{2\sigma_y^2}} \cos(k(x - x_0) - \phi) \ . \tag{7}$$

In this paper, we will use receptive fields of the position-shift type [5,9]: Receptive fields in the right image are shifted by D relative to the left receptive fields. To simplify notation, we set $\phi_{al} = \phi_{ar} = 0$ and use the fact that the receptive field function (7) is separable. Eqs. (1),(2) are then transformed into one-dimensional integrals (using $\sigma := \sigma_x$),

$$S_{al} = \int e^{-\frac{\xi^2}{2\sigma^2}} \cos(k\xi) I_l(\xi)\, d\xi \ , \quad S_{ar} = \int e^{-\frac{(\xi-D)^2}{2\sigma^2}} \cos(k(\xi - D)) I_r(\xi)\, d\xi \ , \tag{8}$$

$$S_{bl} = \int e^{-\frac{\xi^2}{2\sigma^2}} \sin(k\xi) I_l(\xi)\, d\xi \ , \quad S_{br} = \int e^{-\frac{(\xi-D)^2}{2\sigma^2}} \sin(k(\xi - D)) I_r(\xi)\, d\xi \ , \tag{9}$$

where we have defined the one-dimensional images

$$I_{l/r}(\xi) := \int e^{-\frac{(y-y_0)^2}{2\sigma_y^2}} I_{l/r}(\xi + x_0, y) dy \ . \tag{10}$$

The receptive fields of the phase-shift type can be obtained by replacing $\exp(-\frac{(x-x_0-D)^2}{2\sigma^2})$ with $\exp(-\frac{(x-x_0)^2}{2\sigma^2})$ in Eqs. (8) and (9), i.e. the corresponding receptive fields are located in the same positions, but have phase shifts.

2.2 Random Dot Stereo Stimuli

In the following, we do not restrict our derivations to a single stereo stimulus, but rather assume that images are generated by a random process. In the simplest case, each pixel is an identically and independently distributed random variable with mean I_0 and standard deviation σ_I^2. In the continuous limit we will use

$$\langle \bar{I}(\xi) \bar{I}(\xi') \rangle = I_0^2 + \sigma_I^2 \delta(\xi - \xi') \ . \tag{11}$$

We will also assume that the output of the linear filters is zero for an input with constant pixel values (or intensity) over the receptive fields. While this is true for the odd receptive field function, $\int e^{-\frac{\xi^2}{2\sigma^2}} \sin(k\xi) d\xi = 0$, it does not hold exactly for the even function, $\int e^{-\frac{\xi^2}{2\sigma^2}} \cos(k\xi) d\xi = \sqrt{2\pi}\sigma \exp(-\frac{1}{2}k^2\sigma^2)$. This can be accounted for by replacing $\cos(k\xi)$ with $(\cos(k\xi) - \exp(-\frac{1}{2}k^2\sigma^2))$ in Eq. (8). However, in order to simplify the analytical calculations, we do not use this, but ignore constant offsets (which is equal to setting $I_0 = 0$).

We will analyze the case where left and right receptive fields "look" at image parts that are shifted versions of each other, i.e. over the whole receptive field there is a constant disparity d. We do not consider occlusions and variation in depth. However, we take (sensor) noise into account described by identically and independently distributed random variables. Thus, left and right input is modelled as

$$I_l(x) = \bar{I}(x) + \nu_l(x) \ , \qquad I_r(x) = \bar{I}(x-d) + \nu_r(x) \ . \tag{12}$$

Throughout this paper, we will assume $\langle \nu_u(x) \rangle = 0$ and $\langle \nu_u(x)\nu_v(x') \rangle = \sigma_n^2 \times \delta(x-x')\delta_{u,v}$, $u, v \in \{l, r\}$.

Substituting (12) into (8) and (9), and defining $\tilde{d} := d - D$, we obtain

$$S_{al} = \int e^{-\frac{\xi^2}{2\sigma^2}} \cos(k\xi)\bar{I}(\xi)\, d\xi + \int e^{-\frac{\xi^2}{2\sigma^2}} \cos(k\xi)\nu_l(\xi)\, d\xi \ , \tag{13}$$

$$S_{ar} = \int e^{-\frac{(\xi+\tilde{d})^2}{2\sigma^2}} \cos(k(\xi+\tilde{d})\bar{I}(\xi) d\xi + \int e^{-\frac{(\xi-D)^2}{2\sigma^2}} \cos(k(\xi-D))\nu_r(\xi)\, d\xi \ , \tag{14}$$

$$S_{bl} = \int e^{-\frac{\xi^2}{2\sigma^2}} \sin(k\xi)\bar{I}(\xi)\, d\xi + \int e^{-\frac{\xi^2}{2\sigma^2}} \sin(k\xi)\nu_l(\xi)\, d\xi \ , \tag{15}$$

$$S_{br} = \int e^{-\frac{(\xi+\tilde{d})^2}{2\sigma^2}} \sin(k(\xi+\tilde{d}))\bar{I}(\xi)\, d\xi + \int e^{-\frac{(\xi-D)^2}{2\sigma^2}} \sin(k(\xi-D))\nu_r(\xi)\, d\xi \ . \tag{16}$$

2.3 Probability Density Function for the Linear Stage

Since the elements of the vector $\boldsymbol{S} := (S_{al}, S_{ar}, S_{bl}, S_{br})^\top$ are sums of independently and identically distributed random variables, the joint probability density function can be approximated by a Gaussian according to the central limit theorem, i.e.

$$P_{\boldsymbol{S}}(\boldsymbol{S}|\tilde{d}\,) \approx \frac{1}{\sqrt{(2\pi)^4 \det \hat{\boldsymbol{\Sigma}}(\tilde{d}\,)}} \exp(-\tfrac{1}{2}(\boldsymbol{S} - \langle \boldsymbol{S} \rangle)^\top \hat{\boldsymbol{\Sigma}}(\tilde{d}\,)^{-1}(\boldsymbol{S} - \langle \boldsymbol{S} \rangle) \ . \tag{17}$$

As discussed in Sect. 2.2, we assume $\langle \boldsymbol{S} \rangle = \boldsymbol{0}$. The covariance matrix is given by

$$\hat{\boldsymbol{\Sigma}}(\tilde{d}\,) \ = \ \langle (\boldsymbol{S} - \langle \boldsymbol{S} \rangle)(\boldsymbol{S} - \langle \boldsymbol{S} \rangle)^\top \rangle = \langle \boldsymbol{S}\boldsymbol{S}^\top \rangle = \begin{pmatrix} a & c & 0 & e \\ c & a & -e & 0 \\ 0 & -e & b & d \\ e & 0 & d & b \end{pmatrix} \ , \tag{18}$$

$$a := \langle S_{al}^2 \rangle = \langle S_{ar}^2 \rangle = \iint \langle \bar{I}(x)\bar{I}(x') \rangle f_a(x) f_a(x') dx dx' + \sigma_n^2 \int f_a(x)^2 dx \ , \tag{19}$$

$$b := \langle S_{bl}^2 \rangle = \langle S_{br}^2 \rangle = \iint \langle \bar{I}(x)\bar{I}(x') \rangle f_b(x) f_b(x') dx dx' + \sigma_n^2 \int f_b(x)^2 dx \ , \tag{20}$$

$$c := \langle S_{al} S_{ar} \rangle = \iint \langle \bar{I}(x)\bar{I}(x') \rangle f_a(x) f_a(x' + \tilde{d}\,) dx dx' \ , \tag{21}$$

$$d := \langle S_{bl} S_{br} \rangle = \iint \langle \bar{I}(x)\bar{I}(x') \rangle f_b(x) f_b(x' + \tilde{d}\,) dx dx' \ , \tag{22}$$

$$e := \langle S_{al} S_{br} \rangle = -\langle S_{ar} S_{bl} \rangle = \iint \langle \bar{I}(x)\bar{I}(x') \rangle f_a(x) f_b(x' + \tilde{d}\,) dx dx' \ , \tag{23}$$

$$\langle S_{al} S_{bl} \rangle = \langle S_{ar} S_{br} \rangle = 0 \ . \tag{24}$$

By means of the orthogonal 4×4 matrix

$$\hat{\boldsymbol{O}} := \begin{pmatrix} \hat{\boldsymbol{O}}_2 & \boldsymbol{0} \\ \boldsymbol{0} & \hat{\boldsymbol{O}}_2 \end{pmatrix} = \hat{\boldsymbol{O}}^{-1} = \hat{\boldsymbol{O}}^{\top} \quad , \quad \hat{\boldsymbol{O}}_2 := \frac{1}{\sqrt{2}} \begin{pmatrix} 1 & -1 \\ -1 & 1 \end{pmatrix} \quad , \tag{25}$$

we can calculate the probability density function of $\boldsymbol{u} := (u_a, v_a, u_b, v_b)^{\top} = \hat{\boldsymbol{O}}\mathbf{S} = \frac{1}{\sqrt{2}}(S_{al} + S_{ar},\, S_{al} - S_{ar},\, S_{bl} + S_{br},\, S_{bl} - S_{br})^{\top}$,

$$P_{\boldsymbol{u}}(\boldsymbol{u}|\,\tilde{d}) = \frac{1}{\sqrt{(2\pi)^4 \det \hat{\boldsymbol{\Lambda}}(\tilde{d}\,)}} \exp(-\tfrac{1}{2}\boldsymbol{u}^{\top} \hat{\boldsymbol{\Lambda}}(\tilde{d}\,)^{-1}\, \boldsymbol{u}) \quad , \tag{26}$$

$$\text{with } \hat{\boldsymbol{\Lambda}}(\tilde{d}) = \hat{\boldsymbol{O}}\hat{\boldsymbol{\Sigma}}(\tilde{d}\,)\,\hat{\boldsymbol{O}}^{\top} = \begin{pmatrix} a+c & 0 & 0 & -e \\ 0 & a-c & e & 0 \\ 0 & e & b+d & 0 \\ -e & 0 & 0 & b-d \end{pmatrix} \quad . \tag{27}$$

2.4 Non-normalized Complex Cells

According to the energy model, a disparity-tuned complex cell combines the output of two simple cells with orthogonal receptive field functions, i.e.

$$C = S_a^2 + S_b^2 = 2(u_a^2 + u_b^2) \quad . \tag{28}$$

Using

$$P_{u_a u_b}(u_a, u_b|\,\tilde{d}\,) = \iint P_{\boldsymbol{u}}(\boldsymbol{u}|\,\tilde{d}\,) dv_a dv_b = \frac{\exp\big(-\frac{u_a^2}{2(a+c)} - \frac{u_b^2}{2(b+d)}\big)}{\sqrt{4\pi^2(a+c)(b+d)}} \quad , \tag{29}$$

the corresponding probability density function is (for $a + c > b + d$)

$$P_C(C|\tilde{d}\,) = \int_{-\pi}^{\pi} P_{u_a u_b}(\sqrt{C/2}\cos\phi, \sqrt{C/2}\cos\phi|\,\tilde{d}\,)|\det\Big(\frac{\partial(u_a, u_b)}{\partial(C,\phi)}\Big)|d\phi \tag{30}$$

$$= \frac{\exp\big(-\frac{C(a+c+b+d)}{8(a+c)(b+d)}\big)\mathcal{I}_0\big(\frac{C((a+c)-(b+d))}{8(a+c)(b+d)}\big)}{4\sqrt{(a+c)(b+d)}} \quad . \tag{31}$$

$\mathcal{I}_0$ is a modified Bessel function of the first kind.

The mean of complex cell activity ("tuning curve") and its variance are given by

$$\langle C(\tilde{d}\,)\rangle = \int_0^{\infty} C\, P_C(C|\tilde{d}\,)\, dC = 2(a+b+c+d) \quad , \tag{32}$$

$$\mathrm{Var}[C(\tilde{d}\,)] = \langle C^2\rangle - \langle C\rangle^2 = 8(a+c)^2 + 8(b+d)^2 \quad . \tag{33}$$

Eqs. (19)–(23) can be further evaluated for random dot-stimuli,

$$a = \tfrac{1}{2}\sqrt{\pi}\sigma(\sigma_I^2 + \sigma_n^2)\,\big(1 + \exp(-k^2\sigma^2)\big) \quad , \tag{34}$$

$$b = \tfrac{1}{2}\sqrt{\pi}\sigma(\sigma_I^2 + \sigma_n^2)\,\big(1 - \exp(-k^2\sigma^2)\big) \quad , \tag{35}$$

$$c = \tfrac{1}{2}\sqrt{\pi}\sigma\sigma_I^2 \exp\Big(-\frac{\tilde{d}^2}{4\sigma^2}\Big)\,\Big(\cos(k\tilde{d}\,) + \exp(-k^2\sigma^2)\Big) \quad , \tag{36}$$

$$d = \tfrac{1}{2}\sqrt{\pi}\sigma\sigma_I^2 \exp\Big(-\frac{\tilde{d}^2}{4\sigma^2}\Big)\,\Big(\cos(k\tilde{d}\,) - \exp(-k^2\sigma^2)\Big) \quad , \tag{37}$$

$$e = \tfrac{1}{2}\sqrt{\pi}\sigma\sigma_I^2 \exp\Big(-\frac{\tilde{d}^2}{4\sigma^2}\Big)\,\sin(k\tilde{d}\,) \quad . \tag{38}$$

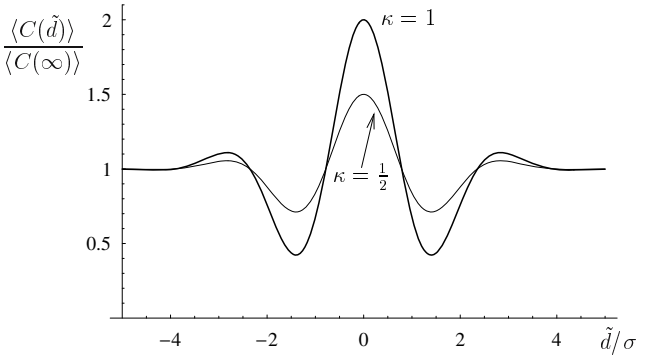

Fig. 2. Tuning curves $\langle C(\tilde{d})\rangle$ of non-normalized complex cells with $k\sigma = 2$ for random-dot stimuli, see Eq. (39). Depth of modulation is $\kappa = 1$ and $\kappa = \frac{1}{2}$ (thin curve). As can be seen from Eq. (40), these curves also show the corresponding standard deviations $\sqrt{\mathrm{Var}[C(\tilde{d})]} \approx \langle C(\tilde{d})\rangle$.

If we assume that $\exp(-k^2\sigma^2) \ll 1$, we can use the approximation $b+d \approx a+c$. A typical value for the visual cortex is $ks \approx 2$, see [10], and thus $\exp(-k^2\sigma^2) \approx \exp(-4) \approx 0.018$.

For the tuning curve of the non-normalized complex cell, we finally have

$$\langle C(\tilde{d})\rangle \approx 4(a+c) = \langle C(\infty)\rangle \Big(\kappa \exp\Big(-\frac{\tilde{d}^2}{4\sigma^2}\Big)\cos(k\tilde{d}) + 1\Big) \ , \qquad (39)$$

where we have defined $\langle C(\infty)\rangle := 2\sqrt{\pi}\sigma(\sigma_I^2 + \sigma_n^2)$ (asymptotic amplitude of complex cell activity for $\tilde{d} \to \infty$) and $\kappa := \frac{\sigma_I^2}{\sigma_I^2+\sigma_n^2}$ ("depth of modulation"). For $\kappa = 1$, Eq. (39) matches the results in [11,12,13]. In addition, we find that the variance of the non-normalized complex cell, Eq. (33), is proportional to the square of the expected response,

$$\mathrm{Var}[C(\tilde{d})] \approx 16(a+c)^2 = \langle C(\tilde{d})\rangle^2 \ . \qquad (40)$$

The probability density function can be approximated for $a + c \approx b + d$ by

$$P_C(C|\tilde{d}) \approx \frac{1}{4(a+c)} \exp\Big(-\frac{C}{4(a+c)}\Big) = \frac{1}{\langle C(\tilde{d})\rangle} \exp\Big(-\frac{C}{\langle C(\tilde{d})\rangle}\Big) \ . \quad (41)$$

Fig. 2 shows tuning curves for $\kappa = 1$ (no noise, $\sigma_n^2 = 0$) and $\kappa = \frac{1}{2}$ (high noise, $\sigma_n^2 = \sigma_I^2$). The corresponding probability density functions, calculated from Eq. (31), are shown in Fig. 3. The maxima at $C = 0$, $\tilde{d}/\sigma \approx 1.5$ correspond to the minima of the tuning curves in Fig. 2.

Except for very high C-values, it is difficult to recognize $\tilde{d} \approx 0$ from the response of the complex cell. This is due to the fact that the complex cell activity

also depends on stimulus contrast. As is shown in the next section, this can be significantly reduced by means of divisive contrast normalization.

2.5 Normalized Complex Cells

In this section we analyze the properties of contrast normalized complex cells. According to Eq. (6) and (4) the normalized complex cell is computed as

$$NC = \frac{(S_{al}+S_{ar})^2+(S_{bl}+S_{br})^2}{(S_{al}^2+S_{ar}^2+S_{bl}^2+S_{br}^2)+\varepsilon} = \frac{2(u_a^2+u_b^2)}{(u_a^2+v_a^2+u_b^2+v_b^2)+\varepsilon} \ . \tag{42}$$

$NC \in [0,2]$ since $v_a^2+v_b^2 \geq 0$.

Using the approximation $b \pm d \approx a \pm c$ that is valid for $\exp(-k^2\sigma^2) \ll 1$, we have

$$\hat{\boldsymbol{\Lambda}}(\tilde{d})^{-1} \approx \frac{1}{a^2-c^2-e^2} \begin{pmatrix} a-c & 0 & 0 & e \\ 0 & a+c & -e & 0 \\ 0 & -e & a-c & 0 \\ e & 0 & 0 & a+c \end{pmatrix} \ . \tag{43}$$

Substituting $(u_a, u_b) = \sqrt{w}(\cos\phi, \sin\phi)$ and $(v_a, v_b) = \sqrt{z}(\cos\psi, \sin\psi)$ the normalized complex cell is given by

$$NC = \frac{2w}{w+z+\varepsilon} \ , \tag{44}$$

and the corresponding probability function can be calculated according to

$$P_{NC}(NC|\,\tilde{d}) = \int_0^\infty\int_0^\infty P_{wz}(w,z)\,\delta\Big(NC - \frac{2w}{w+z+\varepsilon}\Big)dwdz \ , \tag{45}$$

$$\text{with} \quad P_{wz}(w,z|\,\tilde{d}) = \int_{-\pi}^{\pi}\int_{-\pi}^{\pi} \frac{1}{4} P_{\boldsymbol{u}}(w,\phi,z,\psi)d\psi d\phi \tag{46}$$

$$\approx \frac{1}{8\pi A}\int_{-\pi}^{\pi} e^{-\frac{(a-c)w+(a+c)z-2e\sqrt{wz}\sin\phi}{2A}}d\phi \ , \tag{47}$$

with $A := a^2-c^2-e^2$. The delta-function in Eq. (45) ensures that the integration is restricted to the domain where $NC - \frac{2w}{w+z+\varepsilon} = 0$, Eq. (44).

Using $\delta(f(x)) = \sum_i |f'(x_i)|^{-1}\delta(x-x_i)$, where $\{x_i\}$ are the roots of f, we find

$$\delta\Big(NC - \frac{2w}{w+z+\varepsilon}\Big) = \frac{2(z+\varepsilon)}{(2-NC)^2}\,\delta\Big(w - \frac{NC}{2-NC}(z+\varepsilon)\Big) \ , \tag{48}$$

and the integration over w in Eq. (45) yields, with $n := \frac{NC}{2-NC}$,

$$P_{NC}(NC|\,\tilde{d}\,) \approx \frac{2}{(2-NC)^2}\int_0^\infty (z+\varepsilon)P_{wz}\Big(n(z+\varepsilon), z\Big)dz$$

$$= \frac{e^{-\frac{(a-c)n\varepsilon}{2A}}}{4\pi(2-NC)^2A}\int_{-\pi}^{\pi}\int_0^\infty (z+\varepsilon)e^{\frac{2e\sqrt{n(z+\varepsilon)z}\sin\phi-((a-c)n+a+c)z}{2A}}dzd\phi \ . \tag{49}$$

We could not find a way to integrate (49) analytically for $\varepsilon > 0$. However, with the approximation $\sqrt{n(z+\varepsilon)z} \approx \sqrt{n}z$, integration over z and ϕ yields

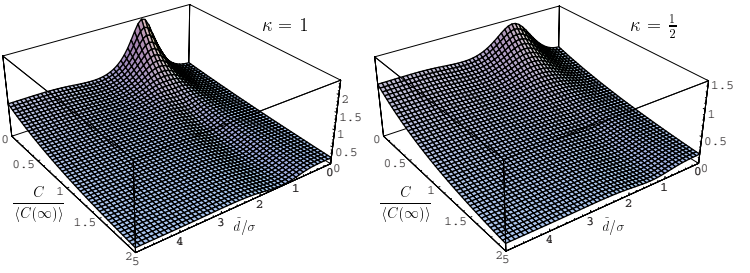

Fig. 3. $P_C(C|\,\tilde{d}\,)$ for $k\sigma = 2$. Because of symmetry, only the range $\tilde{d}/\sigma \geq 0$ is shown.

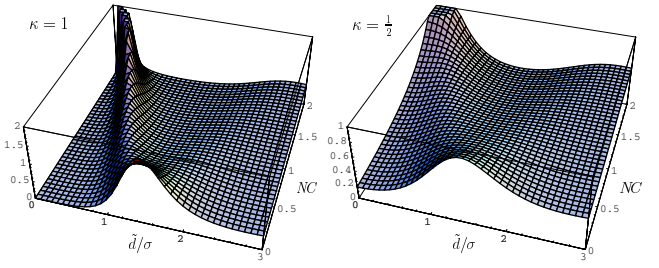

Fig. 4. Probability density functions of normalized complex cells, Eq. (53) for different noise levels, $\kappa = 1 \iff \sigma_n^2 = 0$ and $\kappa = \frac{1}{2} \iff \sigma_n^2 = \sigma_I^2$

$$P_{NC}(NC|\,\tilde{d}\,) \;\approx\; \frac{e^{-\frac{(a-c)NC\varepsilon}{2(2-NC)A}}}{2g[NC]^{\frac{1}{2}}}\Big(\frac{(a+(1-NC)c)A}{g[NC]} + \frac{\varepsilon}{2-NC}\Big)\;, \tag{50}$$

$$\text{with}\quad g[NC] := (a+(1-NC)c)^2 - e^2 NC(2-NC)\;. \tag{51}$$

Eq. (50) is exact for $\varepsilon = 0$, and with $\kappa := \frac{\sigma_I^2}{\sigma_I^2+\sigma_n^2}$ we find

$$P_{NC}(NC|\,\tilde{d};\,\varepsilon=0) = \frac{(a^2-c^2-e^2)(a+(1-NC)c)}{2\big((a+(1-NC)c)^2 - e^2NC(2-NC)\big)^{\frac{3}{2}}} \tag{52}$$

$$= \frac{\big(1-\kappa^2 e^{-\frac{\tilde{d}^2}{2\sigma^2}}\big)\big(1+\kappa(1-NC)e^{-\frac{\tilde{d}^2}{4\sigma^2}}\cos(k\tilde{d})\big)}{2\Big(\big(1+\kappa(1-NC)e^{-\frac{\tilde{d}^2}{4\sigma^2}}\cos(k\tilde{d})\big)^2 - \kappa^2 NC(2-NC)e^{-\frac{\tilde{d}^2}{2\sigma^2}}\sin^2(k\tilde{d})\Big)^{\frac{3}{2}}}\;. \tag{53}$$

Fig. 4 shows the probability density function described by Eq. (53), again for $k\sigma = 2$. Compared to the non-normalized complex cell (see Fig. 3), there is – at least for low noise levels ($\sigma_n^2 \ll \sigma_I^2 \iff \kappa \approx 1$) – a much stronger link between small disparities and high activity ($NC \approx 2$). Thus, if one observes high activity then there is $\tilde{d} \approx 0$ with high probability.

Eq. (53) has simple expressions for the following two cases,

$$\tilde{d} \gg \sigma:\;\; P_{NC}(NC|\,\tilde{d} \gg \sigma;\,\varepsilon=0) \approx \frac{1}{2}\;, \tag{54}$$

$$\tilde{d}=0:\ P_{NC}(NC|\,\tilde{d}=0;\varepsilon=0)=\frac{1-\kappa^2}{2[1+\kappa(1-NC)]^2}\ . \tag{55}$$

In the limit of zero noise, i.e. $\sigma_n^2\to 0$, we find

$$\lim_{\kappa\to 1} P_{NC}(NC|\,\tilde{d}=0;\varepsilon=0)=\delta(2-NC)\ , \tag{56}$$

since $\int_0^2 P_{NC}(NC|\,\tilde{d}=0;\varepsilon=0)\,dNC=1$, and $\lim_{\kappa\to 1} P_{NC}(NC|\,\tilde{d}=0;\varepsilon=0)=0$ for $0\le NC<2$.

Tuning Curve and Variance. The tuning curve is given by

$$\langle NC(\tilde{d}\,)\rangle=\int_0^2 NC\,P_{NC}(NC|\,\tilde{d};\varepsilon=0)\,dNC=1+\cos(k\tilde{d})\kappa e^{-\frac{\tilde{d}^2}{4\sigma^2}}h[\kappa e^{-\frac{\tilde{d}^2}{4\sigma^2}}]\ , \tag{57}$$

$$\text{with}\quad h[u]:=\frac{1}{u^2}-\Big(\frac{1}{u^3}-\frac{1}{u}\Big)\operatorname{artanh}(u)\ . \tag{58}$$

Using $\operatorname{artanh}(u)=\sum_{k=0}^{\infty}\frac{1}{2k+1}u^{2k+1}$, one can show that (for $|u|\le 1$)

$$h[u]=1-\sum_{k=1}^{\infty}\frac{1}{2k+1}\Big(u^{2(k-1)}-u^{2k}\Big)=\sum_{k=0}^{\infty}\Big(\frac{1}{2k+1}-\frac{1}{2k+3}\Big)u^{2k}\ . \tag{59}$$

Since $h[0]=\frac{2}{3}\le h[u]\le h[1]=1$, we obtain

$$\tfrac{2}{3}|\cos(k\tilde{d})|\kappa e^{-\frac{\tilde{d}^2}{4\sigma^2}}\le|\langle NC(\tilde{d})\rangle-1|\le|\cos(k\tilde{d})|\kappa e^{-\frac{\tilde{d}^2}{4\sigma^2}}\ , \tag{60}$$

and for $|\delta|\ll 2\sigma$ the tuning curve can be approximated by

$$\langle NC(\tilde{d})\rangle\approx 1+\cos(k\tilde{d})\kappa e^{-\frac{\tilde{d}^2}{4\sigma^2}}\ . \tag{61}$$

Since $\langle C(\tilde{d})\rangle/\langle C(\infty)\rangle=\cos(k\tilde{d})\kappa e^{-\frac{\tilde{d}^2}{4\sigma^2}}$, we find that normalized and non-normalized complex cell have similar tuning curves – as can be seen in Fig. 5. The approximation $\langle NC(\tilde{d})\rangle\approx 1+\frac{2}{3}\kappa\cos(k\tilde{d})e^{-\frac{\tilde{d}^2}{4\sigma^2}}+\frac{1}{3}\kappa^3\cos(k\tilde{d})e^{-\frac{3\tilde{d}^2}{4\sigma^2}}$ has been obtained using the first three terms in Eq. (59), i.e. $h[u]\approx\frac{2}{3}+\frac{1}{3}u^2$.

Using

$$\langle NC(\tilde{d})^2\rangle:=\int_0^2 NC^2\,P_{NC}(NC|\,\tilde{d};\varepsilon=0)\,dNC\ , \tag{62}$$

the variance in the response of the non-normalized complex cell is

$$\operatorname{Var}[NC(\tilde{d})]\ =\ \langle NC(\tilde{d})^2\rangle-\langle NC(\tilde{d})\rangle^2=(1-\kappa^2e^{-\frac{\tilde{d}^2}{2\sigma^2}})H[\kappa^2e^{-\frac{\tilde{d}^2}{4\sigma^2}},k\tilde{d})]\ , \tag{63}$$

$$\text{with } H[u,v]:=(\cos^2v-\sin^2v)\frac{1}{u^2}+\sin^2v\frac{1}{u^3}\operatorname{artanh}(u)\ . \tag{64}$$

One can show that $\frac{1}{3}(1-\kappa^2e^{-\frac{\tilde{d}^2}{2\sigma^2}})<\operatorname{Var}[NC(\tilde{d})]<\frac{1}{3}$.

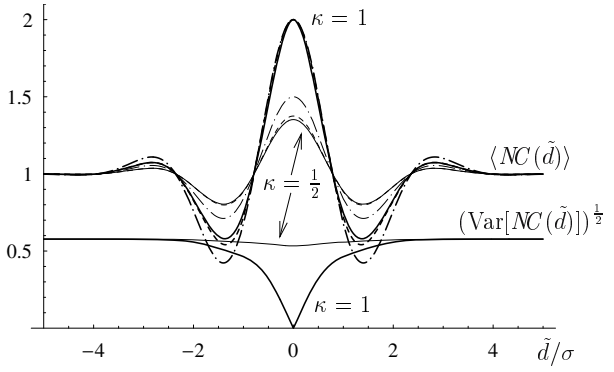

Fig. 5. Tuning curve $\langle \mathcal{NC}(\tilde{d})\rangle$ of the normalized complex cell (continuous curve), Eq. (57), and the approximations $1+\kappa\cos(k\tilde{d})e^{-\frac{\tilde{d}^2}{4\sigma^2}} = \langle C(\tilde{d})\rangle/\langle C(\infty)\rangle$ (dash-dotted), and $1+\frac{2}{3}\kappa\cos(k\tilde{d})e^{-\frac{\tilde{d}^2}{4\sigma^2}}+\frac{1}{3}\kappa^3\cos(k\tilde{d})e^{-\frac{3\tilde{d}^2}{4\sigma^2}}$ (dashed), for $k\sigma = 2$. The noise levels are $\sigma_n^2 = 0$ ($\kappa = 1$, bold curves) and $\sigma_n^2 = \sigma_I^2$ ($\kappa = \frac{1}{2}$, thin curves). The dash-dotted curves are identical to the curves in Fig 2. Also shown is the standard deviation $(\mathrm{Var}[\mathcal{NC}(\tilde{d})])^{\frac{1}{2}}$.

By means of Taylor expansion of $\mathrm{artanh}(u)$, we have found a good approximation, $\mathrm{Var}[\mathcal{NC}(\tilde{d})] \approx (1-\kappa^2 e^{-\frac{\tilde{d}^2}{2\sigma^2}})\Big(\frac{1}{3}+\kappa^2 e^{-\frac{\tilde{d}^2}{2\sigma^2}}[\frac{1}{5}\sin^2(k\tilde{d})+\frac{7}{45}\cos^2(k\tilde{d})]\Big)$.

Fig. 5 also shows the standard deviation $(\mathrm{Var}[\mathcal{NC}(\tilde{d})])^{1/2}$ for zero noise ($\kappa = 1$) and strong noise ($\sigma_n^2 = \sigma_I^2$, $\kappa = \frac{1}{2}$). The low variance for small $\tilde{d}$ (and low noise) enhances the detectability of stimulus disparities D that are close to the neuron's preferred disparity d (compare with Fig. 2 and $\mathrm{Var}[C(\tilde{d})] \approx \langle C(\tilde{d})\rangle^2$).

3 Comparing Analytical Results with Simulations

As a control of the analytically derived results we performed computer simulations with discrete images and applied circular Gabor filters of bandwidth two, more specifically we set $\sigma_x = \sigma_y = 5/2\,\mathrm{pixel}$ and $k = 2/3\,\mathrm{pixel}^{-1}$. The (separable) 2D Gabor filters are approximated by two pairs of row and column filters. The size of these filters is 13×1 and 1×13 (corresponding to a 13×13 filter mask in 2D), and their elements are integer values. As "stimuli" we used random dot images consisting of black and white pixels. Disparities were simulated by shifting the right image with respect to the left image. For each disparity, mean and standard deviation of complex cells were computed. As can be seen in Fig. 6, the analytically derived equations fit the data quite well.

4 Discussion, Limitations of the Model

We have shown analytically that simple contrast normalization can greatly enhance disparity detection for binocular neurons of the energy type. While the

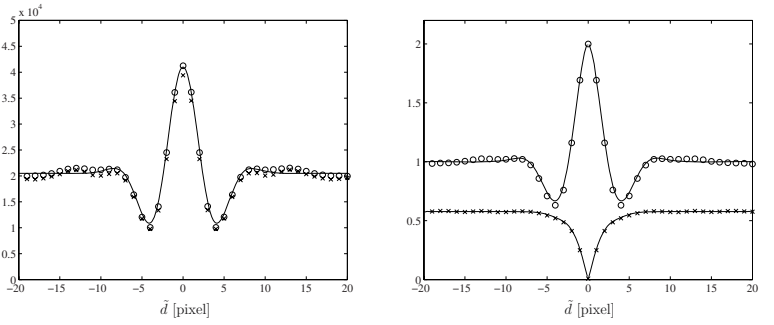

Fig. 6. Simulated disparity tuning curves (circles) and standard deviation (crosses) for non-normalized complex cell (left) and normalized complex cell (right). The continuous curves show the analytical results, Eqs. (39),(40) and (57),(63) respectively.

"classical" model predicts that the standard deviation is proportional to the mean firing rate for random-dot stimuli, divisive normalization significantly reduces the standard deviation, in particular close to the preferred disparity. The simple expression for contrast normalization given by Eq. (6) has been chosen in order to make analytical calculations more convenient. For the same reason, i.e. to keep the model simple, monocular normalization which is known to play a major role in gain control [14], was not included. In addition, although we have taken sensor noise (with constant variance) into account, our model does not include intrinsic response variability of the disparity tuned neuron. This has to be considered when comparing the calculated variances to measured data. Response variances to dynamic random dot stimuli have been reported to be approximately proportional to the mean firing rate [15,16].

References

1. Ohzawa, I., DeAngelis, G., Freeman, R.: Stereoscopic depth discrimination in the visual cortex: Neurons ideally suited as disparity detectors. Science 249, 1037–1041 (1990)
2. Adelson, E., Bergen, J.: Spatiotemporal energy models for the perception of motion. J. Opt. Soc. Am. A 2, 284–299 (1985)
3. Anzai, A., Ohzawa, I., Freeman, R.: Neural mechanisms for processing binocular information. I. Simple cells. J. Neurophysiol. 82, 891–908 (1999)
4. Anzai, A., Ohzawa, I., Freeman, R.: Neural mechanisms for processing binocular information. II. Complex cells. J. Neurophysiol. 82, 909–924 (1999)
5. Fleet, D., Heeger, D., Wagner, H.: Modeling binocular neurons in primary visual cortex. In: Jenkin, M., Harris, L. (eds.) Computational and Biological Mechanisms of Visual Coding, pp. 103–130. Cambridge University Press, Cambridge (1996)
6. Heeger, D.: Normalization of cell responses in cat striate cortex. Vis. Neurosci. 9, 181–197 (1992)
7. Carandini, M., Heeger, D., Movshon, J.A.: Linearity and normalization in simple cells of the macaque primary visual cortex. The Journal of Neuroscience 17, 8621–8644 (1997)

8. Wainwright, M., Schwartz, O., Simoncelli, E.: Natural image statistics and divisive normalization: Modeling nonlinearity and adaptation in cortical neurons. In: Rao, R., Olshausen, B., Lewicki, M. (eds.) Probabilistic Models of the Brain: Perception and Neural Function, MIT Press, Cambridge (2002)
9. Anzai, A., Ohzawa, I., Freeman, R.: Neural mechanisms for encoding binocular disparity: Receptive field position versus phase. J. Neurophysiol. 82, 874–890 (1999)
10. DeValois, R., DeValois, K.: Spatial Vision. Oxford University Press, Oxford (1988)
11. Zhu, Y., Qian, N.: Binocular receptive field models, disparity tuning, and characteristic disparity. Neural Computation 8, 1611–1641 (1996)
12. Tsai, J., Victor, J.: Reading a population code: a multi-scale neural model for representing binocular disparity. Vision Research 43, 445–466 (2003)
13. Tanabe, S., Doi, T., Umeda, K., Fujita, I.: Disparity-tuning characteristics of neuronal responses to dynamic random-dot stereograms in macaque visual area V4. J. Neurophysiol. 94, 2683–2699 (2005)
14. Truchard, A., Ohzawa, I., Freeman, R.: Contrast gain control in the visual cortex: Monocular versus binocular mechanisms. The Journal of Neuroscience 20, 3017–3032 (2000)
15. Read, J., Cumming, B.: Testing quantitative models of binocular disparity selectivity in primary visual cortex. J. Neurophysiol. 90, 2795–2817 (2003)
16. Prince, S., Pointon, A., Cumming, B., Parker, A.: Quantitative analysis of the responses of v1 neurons to horizontal disparity in dynamic random-dot stereograms. J. Neurophysiol. 87, 191–208 (2002)